ResearchGate

See discussions, stats, and author profiles for this publication at: https://www.researchgate.net/publication/231651958

One-Pot Synthesis of Gold Nanoshells with High Photon-to-Heat Conversion Efficiency

ARTICLE *in* THE JOURNAL OF PHYSICAL CHEMISTRY C · APRIL 2009

Impact Factor: 4.77 · DOI: 10.1021/jp810544b

CITATIONS
27

READS
54

5 AUTHORS, INCLUDING:

Barbara Storti
Scuola Normale Superiore di Pisa
17 PUBLICATIONS **271** CITATIONS
SEE PROFILE

Fausto Elisei
Università degli Studi di Perugia
193 PUBLICATIONS **3,420** CITATIONS
SEE PROFILE

Stefania Abbruzzetti
Università degli studi di Parma
75 PUBLICATIONS **1,393** CITATIONS
SEE PROFILE

Loredana Latterini
Università degli Studi di Perugia
120 PUBLICATIONS **2,232** CITATIONS
SEE PROFILE

Available from: Loredana Latterini
Retrieved on: 31 January 2016

THE JOURNAL OF PHYSICAL CHEMISTRY C

Subscriber access provided by UNIVERSITA DI PERUGIA

Article

One-Pot Synthesis of Gold Nanoshells with High Photon-to-Heat Conversion Efficiency

Barbara Storti, Fausto Elisei, Stefania Abbruzzetti, Cristiano Viappiani, and Loredana Latterini

J. Phys. Chem. C, **2009**, 113 (18), 7516-7521• Publication Date (Web): 08 April 2009

Downloaded from http://pubs.acs.org on April 30, 2009

More About This Article

Additional resources and features associated with this article are available within the HTML version:

- Supporting Information
- Access to high resolution figures
- Links to articles and content related to this article
- Copyright permission to reproduce figures and/or text from this article

View the Full Text HTML

ACS Publications
High quality. High impact.

The Journal of Physical Chemistry C is published by the American Chemical Society. 1155 Sixteenth Street N.W., Washington, DC 20036

One-Pot Synthesis of Gold Nanoshells with High Photon-to-Heat Conversion Efficiency

Barbara Storti,[†,§] Fausto Elisei,[†] Stefania Abbruzzetti,[‡] Cristiano Viappiani,[‡] and Loredana Latterini*[,†]

Dipartimento di Chimica and Centro di Eccellenza Materiali Innovativi Nanostrutturati (CEMIN)—Università di Perugia, Via Elce di Sotto, 8, 06123 Perugia, Italy, and Dipartimento di Fisica, Università degli Studi di Parma, CNISM, and NEST CNR-INFM, Viale G. P. Usberti 7A, 43100 Parma, Italy

Received: December 1, 2008; Revised Manuscript Received: March 10, 2009

A new one-pot method for the preparation of gold nanoshells on amino-functionalized silica nanoparticles is presented together with the determination of their heat release efficiency. The synthesis of silica nuclei and the growth of a thin gold capping layer was done in the same pot; upon controlling the experimental conditions, it was possible to keep the final diameter of the hybrid nanoparticles below 30 nm, with a gold layer of 6 nm. Photoacoustic measurements carried out on gold nanoshell suspensions demonstrate that heat release occurs with an efficiency close to unity, regardless of the chemical nature of the stabilizer on the gold surface. The effectiveness of gold nanoshells in converting photons into heat has been tested by inducing thermal denaturation of nanoshell-coupled EGFP (enhanced green fluorescent protein). These measurements indicate that the thermal effects detected in gold nanostructures are long-range phenomena, which are potentially useful in photothermal treatments, but should be taken into account when designing gold-based devices or using gold surfaces to enhance optical signals.

Introduction

Metal nanostructures have in recent years attracted much attention due to their electronic properties,[1−3] which can be tuned and controlled during the synthesis.[4−7] Generally, noble metal nanostructures support a collective oscillation of the conduction electrons in the visible range of the electromagnetic spectrum, known as surface plasmon resonance (SPR), whose frequency strongly depends on the size, shape, composition, and environment of the particle.[8,9] This nanosize effect stimulated the use of metal nanoparticles in different fields such as surface enhancement spectroscopies,[10−12] waveguides[13] and sensors.[14−16] Due to low gold toxicity, gold nanoparticles are particularly interesting for biomedical applications which include photothermal imaging[17−22] and tumor photothermal treatment.[23−25] For these uses, it is convenient to shift the SPR band in the red/NIR region where the tissue light absorbed fraction is negligible.[26]

Gold nanoshells, consisting of a thin gold layer around a dielectric nucleus (silica), are generally prepared via a three step method in which the synthesis of silica nuclei, their functionalization, and the growth of the gold layer were accomplished in distinct phases.[27] Although simple, this preparation method is quite plodding and prevents scaling of the procedure. When the gold shell is complete, the nanostructures show an intense NIR absorption which was used for *in vivo* photothermal cell treatments.[28] Despite many research efforts, several questions on gold nanoshells are still open. While it is known that the electronic properties of gold nanoshells are dependent on the surrounding media,[8] a quantitative estimate of the medium effects on the photothermal conversion efficiency is still missing. Furthermore, it remains to be understood whether the heat released by gold nanoshells is converted in a bulk effect or it is dissipated near the nanoshell (long or short distance effect, respectively) and if this is of relevance to different applications such as *in vivo* photothermal treatments and biosensors. This information will give new insight for application of these nanostructures in material science (photonic devices, solar cells, etc.) or to promote localized conformational changes in biodevices.

In the present work, a new, one-pot preparation procedure has been developed, which reduces the preparation commitment, since the growth of gold nanoshells and the synthesis of amino-functionalized silica nanoparticles, used as nuclei, was carried out in the same pot. We show that the excess energy of the gold nanoshells after photoexcitation is rapidly released as heat with unit efficiency, hinting at perspective applications in cell photothermal treatments and warning against photothermal side effects in photonic applications.

Experimental Section

Chemicals. Tetrachloroauric(III) acid ($HAuCl_4 \cdot 3H_2O$, ≥99.9%) and 3-aminopropyl-triethoxysilane (APTES, 99%) were purchased from Aldrich. Citric acid trisodium salt dihydrate (sodium citrate, ≥99.0%) was from Fluka. All chemicals were used without any further purification procedures. Milli-Q water was used as solvent.

Preparation of Silica Nanoparticles Gold Nanoshells. Synthesis of amino-functionalized silica nuclei was achieved by hydrolysis of (3-aminopropyl)triethoxysilane (APTES) in aqueous solution at pH values below 2.[29] An acidic solution of APTES in water (volume ratio 0.007) was vigorously stirred for about 30 min and then poured in a sodium citrate water solution (5×10^{-3} M). Upon adjusting the reactant concentration and the reaction time, a controlled condensation process occurs,

* To whom correspondence should be addressed. E-mail: loredana@unipg.it. Telephone: +390755855636. Fax: +390755855598.
† Università di Perugia.
‡ Università degli Studi di Parma, CNISM, and NEST CNR-INFM.
§ Present address: Scuola Normale Superiore, Laboratorio NEST—Complesso San Silvestro, Piazza San Silvestro, 12-56127 Pisa, Italy.

10.1021/jp810544b CCC: $40.75 © 2009 American Chemical Society
Published on Web 04/08/2009

leading to the formation of nanometer-sized amino-functionalized silica particles (AF-Si nanoparticles). The amino groups are pointing toward the aqueous environment, as can be deduced by the pH-dependent aggregation observed upon increasing the pH above 7.5.[30]

The AF-Si nanoparticles were used without further treatments as nuclei to build up gold nanoshells using the redox reaction previously reported in the literature.[25] For this purpose, the sodium citrate solution was added to the suspension of AF-Si nanoparticles and heated at 100 °C. Twenty milliliters of a $HAuCl_4 \cdot 3H_2O$ (6×10^{-4} M) solution in Milli-Q grade water was slowly added. Under these conditions, the reduction of Au^{3+} by sodium citrate leads to the nucleation of Au particles which were coordinated on the silica surface by the amino groups. Afterward, the suspension was kept at 60 °C for about 30 min to allow the growth of the gold layer to reach a complete shell on the silica nucleus, as deduced from the optical absorption properties (*vide infra*).

Optical Characterization. UV−vis absorption spectra were recorded with a double beam Perkin-Elmer Lambda 800 spectrophotometer.

Irradiation Procedure. The photostability test was performed by monitoring the absorption spectra as a function of irradiation time (λ_{exc} = 530, 650, and 850 nm, bandwidth 10 nm, for CW and λ_{exc} = 532 nm for pulsed irradiation) using a solution of gold nanoshells with 0.4 absorption at the excitation wavelength. Irradiation was performed with a 450 W xenon lamp or with a Nd:YAG laser (Continuum, Surelite II-10, pulse width ca. 7 ns and energy ≤10 mJ pulse^{-1}). Under the different experimental conditions, the energy introduced on the samples was about 1.5 J/cm^2.

Transmission Electron Microscopy (TEM). A Philips model 208 transmission electron microscope (operating at 80 kV of beam acceleration) was used to analyze the size and size distribution of the nanoparticles and gold nanoshells. Nanoparticles (or nanoshells) dissolved in Milli-Q water were deposited in a 400 mesh copper coated with a Formvar support grid and left overnight in a desiccator to let the solvent evaporate. The size distribution histograms for the samples were obtained by analyzing 150−200 nanoparticles (or nanoshells) in each sample.

Atomic Force Microscopy (AFM). An atomic force microscope (Solver-Pro P47H, NT-MDT) was used to record topography and phase images of nanoparticles and nanoshells. The measurements were carried out under semicontact conditions by use of a 190−325 kHz cantilever having super sharp diamond-like carbon tips with a typical curvature radius of 1 nm (NT-MDT), which allows us to reach about 0.8 nm in height resolution, as tested with standard samples. A drop of the sample suspended in water was placed on mica and spin coated in order to spread the solution and render the solvent easily evaporable. A grain analysis was carried out to determine the size distribution of the particles from the images. The size distribution histograms for the samples were obtained by analyzing 150−200 nanoparticles (or nanoshells) in each sample.

Time-Resolved Photoacoustics. The experimental setup has been described previously.[31,32] Photoexcitation was achieved by the second harmonic (λ_{ex} = 532 nm) of a nanosecond Q-switched Nd:Yag laser (Surelite II-10 Continuum). The unfocused beam was attenuated and shaped by a 280 μm slit positioned near the cuvette. The pressure wave induced in the solution was detected by a PZT piezoelectric transducer (Panametrics V-103). The signal was then amplified (60 dB) and recorded with a digitizing oscilloscope (LeCroy 9450A) operated at 2.5 ns/channel. A quartz cuvette was mounted inside a temperature controlled sample holder (Quantum Northwest, Inc. TASC 300) and degassed with nitrogen. Data acquisition and analysis were performed by means of dedicated software (Sound Acquisition and Sound Analysis, Quantum Northwest, Inc.). 100 laser shots were averaged to generate each reference and sample waveform. The sample was stirred periodically to avoid precipitation of the nanoshells. The energy entering the sample was about 20 μJ. Brilliant Black BN (BBBN) (Aldrich) was used as photocalorimetric reference compound.[33] The reference solution contained uncoated silica nanoparticles at the same concentration to match the thermoelastic properties of the sample solutions.[34−36] The absorbance of the nanoshells aqueous solutions was kept around 0.4 cm^{-1} at the excitation wavelength and matched the absorbance of the reference compound solution.

The principles of deconvolution of photoacoustic waveforms have been described.[37,38] The best fit was obtained with a single exponential decay with a lifetime below the experimental resolution (≈20 ns). The possible presence of structural volume changes was checked using a two-temperature method.[35] The sample waveform was acquired at $T_{\beta=0}$ (the temperature at which the thermal expansion coefficient β vanishes), which, for the solvent used, was identical to that of pure water (3.9 °C). This waveform was compared to a reference waveform acquired at a slightly higher temperature (7 °C). No pure volumetric signal was detected, thus showing that the measured signal has a pure enthalpic origin. We can thus write for the amplitude φ of the photoacoustic signal:

$$\varphi = \frac{Q}{E_\lambda}$$

where φ is the pre-exponential factor retrieved from the deconvolution analysis, E_λ is the molar energy content of the laser pulse, and Q is the heat released in the deexcitation.

Fluorescence Correlation Spectroscopy. Fluorescence correlation spectroscopy (FCS) experiments were performed using a Microtime 200 from Picoquant, based on an inverted confocal microscope (Olympus IX70) and equipped with two SPADs (single photon avalanche diodes) used in the cross-correlation mode. Excitation was achieved by a 475 nm picosecond diode laser, and fluorescence emission by the enhanced green fluorescent protein (EGFP; mutations F64L, S65T) was split with a 50/50 splitter between the two detection channels and collected through matched bandpass filters (AHF, SMDEmitter HQ 520/40). The EGFP concentration was kept at 50 nM in all of the experiments.

The same setup allowed the determination of fluorescence decays of EGFP either free in solution or complexed to the nanoshells under the same experimental conditions used in the FCS experiments.

EGFP was complexed to the gold coated nanoshells with a 50 nM final concentration in a solution of absorbance 0.4 at 532 nm. The solutions contained 1 mM phosphate buffer at neutral pH. The solution was allowed to equilibrated for 24 h, after which time complexes between the proteins and the gold nanoshells are formed. Under these experimental conditions, only a few molecules (always below 10) were detected in the confocal volume.

Results

The morphology and size of AF-Si nanoparticles was investigated by transmission electron microscopy (TEM) and atomic force microscopy. Figure 1 shows a representative TEM image of AF-Si nanoparticles. Analysis performed on this and similar images shows that the particles we obtained have indeed

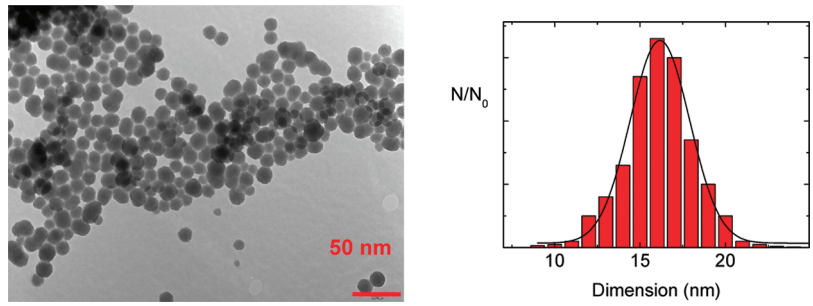

Figure 1. TEM image of amino-functionalized particles (AF-Si) together with size distribution.

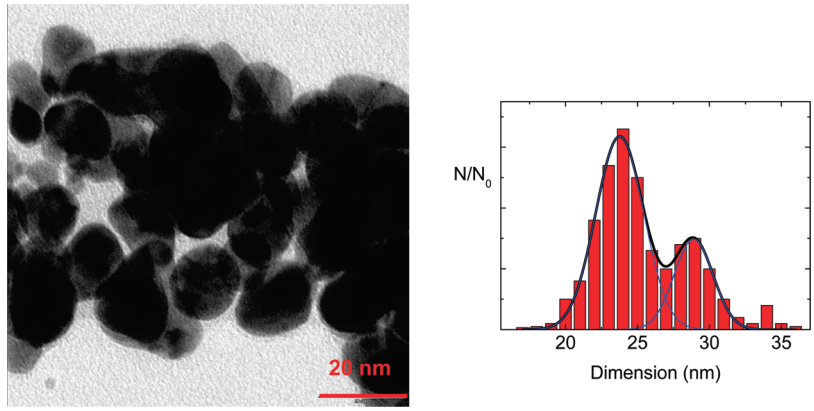

Figure 2. TEM image of gold coated amino-functionalized particles together with size distribution.

nanometer-size with a diameter of 16 ± 3 nm and good monodispersion. AFM images present a regular surface without roughness or defects (Figure 3).

Gold nanoshells were grown starting from the AF-Si nanoparticles as outlined in the Experimental Section. The growth of the shell was checked by TEM imaging. Figure 2 shows a representative image taken at the end of the growth process. The nanoparticles appeared completely coated with a metal shell, as indicated by the contrast distribution and the absence of seeds accumulation, which is normally observed when the shell growth is not complete.[8] It has to be noted that deviation from perfectly round shapes can be observed in some particles, as compared to the starting AF-Si structures, suggesting that in the present conditions a preferential axial growth of the shell occurred, which can account for the different contrast levels observed in the image of Figure 2. The metal layer dimension was determined by comparison between the size distribution before and after gold treatment. In particular, the diameter distribution of the gold nanoshells, determined from the analysis of images similar to that reported in Figure 2, is well described by two Gaussian distributions with peaks at 24 ± 3 and 29 ± 3 nm, indicating the presence of two subpopulations of gold nanoshells. We associate the lower diameter population with those nanoshells for which a complete gold shell around the AF-Si nucleus has grown. The larger diameter observed in the second population is likely due to the deposition of a second partial gold layer in some particles (since the diameter difference between the two populations is similar to the gold seeds, about 5 nm). AFM images confirmed the dimensions increase of the nanoparticles and revealed a smooth surface of the gold nanoshells, suggesting the formation of a complete shell (Figure 3). Differently from what previously was observed for similar systems,[39] no roughness could be detected within the instrumental resolution, suggesting that no accumulation of small gold particles occurred on the silica surface. On the other hand, incomplete shell formation and the presence of gold seeds stuck on the silica surface were observed at the early stages of gold layer growth (Supporting Information). Further support for complete shell formation for mature nanoshells comes from the changes in the absorption spectra recored at different reaction times, which show a broadening of the SPR peak at 525 nm until its disappearance (Supporting Information).

The optical properties of the gold nanoshell suspensions were monitored in the 350−1100 nm range. Their absorption spectra presented a broad band in the 500−1100 nm region, in agreement with literature data reported for gold nanoshells,[12] with a broad and structureless maximum at 800 nm. The spectrum is much broader than the calculated ones,[1,40] likely due to the presence of deviations from the spherical shape. The gold nanoshells proved stable for at least two months, according to the good reproducibility with time of the absorption spectra and the TEM images.

In view of the potential application in photothermal treatments (*vide infra*), the photostability of the gold nanoshells is an important issue. Upon CW or pulsed irradiation of the gold nanoshell suspensions, their absorption spectra did not significantly change (Figure 4), thus indicating a good photochemical stability. Irradiation with higher radiation fluence (about 15 J/cm^2) resulted in a decrease of the absorption intensity, which is at the moment under investigation.

We then used time-resolved photoacoustic measurements to quantify the heat release efficiency after photoexcitation.[36] Nanosecond photoexcitation at 532 nm of a solution containing gold nanoshells afforded photoacoustic signals which were almost undistinguishable from those obtained with the photocalorimetric reference compound, with an amplitude of 0.97 ± 0.05. Since no photoinduced structural volume changes were detected, this result shows that, after absorption of a photon,

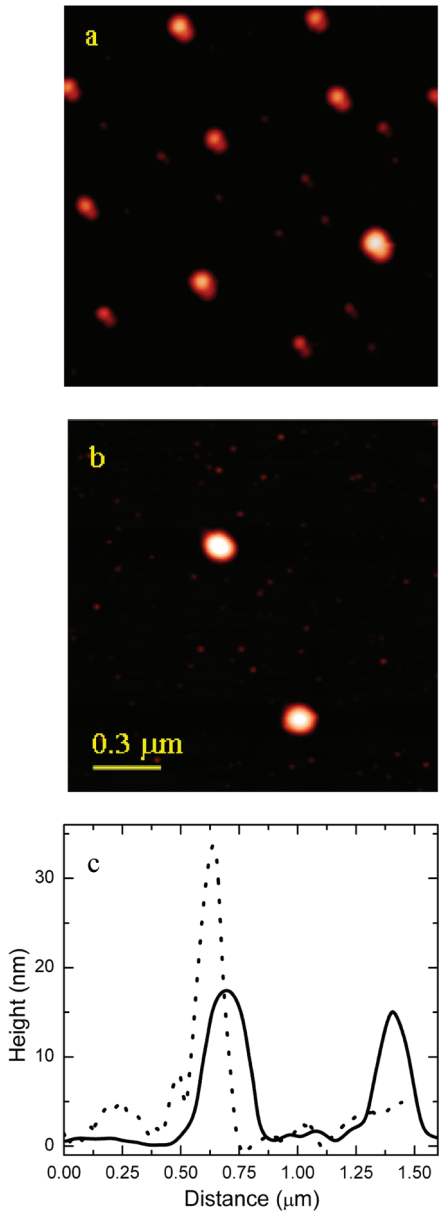

Figure 3. AFM images of (a) amino-functionalized particles (AF-Si) and (b) gold coated amino-functionalized particles (scale bar corresponds to 0.3 μm for both the images) together with line scan profiles (c) recorded from image a (full line) and image b (dashed line).

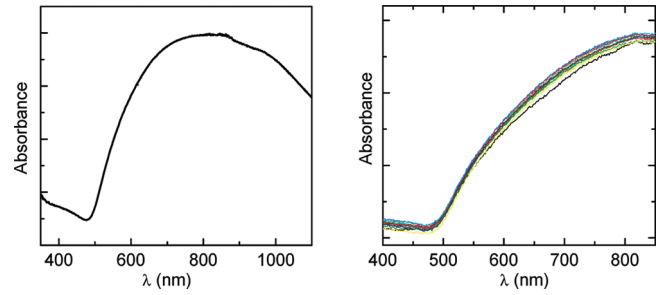

Figure 4. Absorption spectrum of gold coated amino-functionalized particles recorded at the end of reaction process (left panel) and at different irradiation times at $\lambda = 532$ nm (right panel), from 0 (black curve, before irradiation) to 180′ (cyan curve, after irradiation with 1.5 J/cm^2).

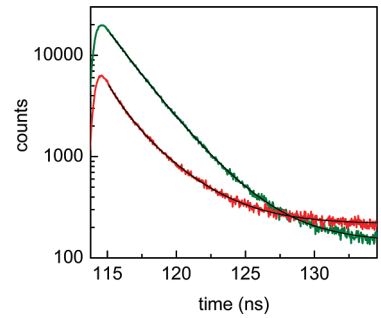

Figure 5. Fluorescence decay signals from EGFP (green) and EGFP complexed to gold nanoshells (red) ($\lambda_{exc} = 475$ nm) together with double exponential fitting curves (black).

all of the absorbed energy is quickly (below the instrumental resolution, 20 ns) released as heat. Attempts to monitor optical transients with nanosecond laser flash photolysis and transient absorbance failed to detect any signal in the 400−800 nm spectral range, in agreement with literature data.[41] Similar photoacoustic signals were obtained upon excitation of the gold nanoshells at 1064 nm. These findings indicate the possibility to convert plasmonic effects localized in nanometer objects to a bulk effect, since the light absorbed by the gold nanoshells is transformed into heat recorded by the acoustic detector without any losses, at least at the excitation fluence used in the present measurements. Quantification of the process in terms of a temperature gradient produced in correlation with the gold nanoshells' concentration is currently under investigation with the idea to reach a plasmon assisted temperature control in the bulk, as already reported for nanometer-scale systems.[42] Similar results were obtained when changing the stabilizer at the nanoshell surfaces. In particular, when citrate anions were replaced by *O*-[2-(3-mercaptopropionylamino)ethyl]-*O*′-methylpolyethylene glycol or by ribonuclease A, the efficiency in heat release did not change significantly, thus suggesting that the nature of the capping agent does not alter the photophysical behavior of the particles, differently from what was observed for the plasmonic resonances.[8,9]

The capability of gold nanoshells to introduce substantial heating in their immediate surroundings was further demonstrated by inducing thermal denaturation of nanoshell-bound EGFP. To avoid the interference of unbound protein molecules, the nanoparticle−EGFP suspensions were allowed to equilibrate for 24 h, and proteins−gold nanoshells complexes could be formed; although the nature of interactions between nanoshells and EGFP was not investigated at this stage, it is likely that electrostatic forces (driven by acid−base centers of the nanoshell stabilizer) play an important role in assisting complex formation.

Time-resolved fluorescence emission of EGFP solutions (Figure 5) was well described by a double exponential relaxation with lifetimes of 1.9 ns (45%) and 2.9 ns, in agreement with literature data.[43] Addition of increasing concentrations of gold nanoshells resulted in evident quenching of EGFP emission. The protein fluorescence intensity was significantly decreased with only minor changes to the lifetimes (1.2 ns (46%) and 3.2 ns), indicating that static quenching is mainly occurring. Solutions containing only nanoshells gave fluorescence signals undistinguishable from those of the background; thus, no fluorescence contamination from the nanoshells is responsible for the observed fluorescence emission decays.

Further indications that coupling of EGFP to the nanoshells has occurred come from the analysis of the fluorescence correlation spectroscopy (FCS) curves. Figure 6 compares the

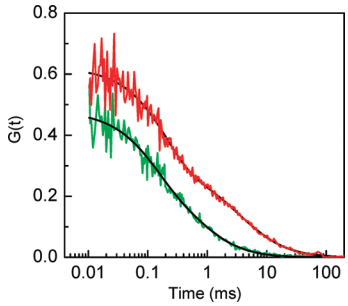

Figure 6. Fluorescence cross-correlation functions for neutral aqueous solutions of EGFP (green) and EGFP complexed to gold nanoshells (red). Black curves are fittings to a model previously proposed for EGFP, taking into account diffusion and exchange of protons with the solvent.[44]

FCS signals measured for an EGFP solution and a solution containing 50 nM EGFP complexed to the gold coated nanoshells. The diffusional part of the FCS decay becomes slower upon binding of the protein to the nanoshells, in agreement with the expected slower diffusion due to the larger size of the complex. Analysis of the FCS curves with a model taking into account the protonation equilibrium of the chromophore and the diffusional motion[44] afforded a diffusion coefficient of 90 $\mu m^2/s$ for EGFP, in agreement with previous determinations (78 $\mu m^2/s$).[45] When EGFP was complexed with the nanoshells, the diffusion coefficient dropped to about 15 $\mu m^2/s$, with this 6-fold reduction being consistent with the 6-fold increase in diameter of the diffusing species.

In order to show the effectiveness of gold coated nanoshells in conveying the absorbed photon energy into heat, we have exposed the solutions to greatly attenuated 1064 nm laser pulses from a nanosecond Nd:YAG laser and monitored the effects on the signals from EGFP (lifetimes and FCS) in the presence and in the absence of gold nanoshells. Photoexcitation with a single 1064 nm (5 ns) laser pulse of a suspension of EGFP-nanoshells led to complete disappearance of the fluorescence signal from EGFP, even at the lowest reliably achievable pulse energy (1 mJ, $\approx$0.3 MW/cm^2), showing that thermal denaturation of the protein had been achieved. When EGFP solutions were exposed to laser pulses of the same power density, no appreciable changes in fluorescence emission or in the fluorescence cross-correlation function were detected, showing that the proteins were damaged only when complexed to the gold nanoshells.

Conclusions

The simplified preparation method we propose makes it feasible to obtain nanometer sized silica−gold hybrid particles with a broad surface plasmon resonance band. Upon photoexcitation of the gold nanoshells, heat release efficiency close to unity was measured. The effectiveness of gold nanoshells in converting photons into heat was further demonstrated by inducing thermal denaturation of nanoshell-coupled EGFP. These measurements indicate that the thermal effects detected in metal nanostructures could be potentially exploited in photothermal treatments and should not be neglected when these structures are used with different purposes, e.g., within photonic devices.

Acknowledgment. The authors thank Dr. T. Gensch for useful discussions and for providing the EGFP sample and Dr. Matteo Amelia for technical support. The Ministero per l'Università e la Ricerca Scientifica e Tecnologica (Rome) is acknowledged for financial support.

Supporting Information Available: TEM images and absorption spectra of incomplete nanoshells. This information is available free of charge via the Internet at http://pubs.acs.org.

References and Notes

(1) Schatz, G. C. *Proc. Natl. Acad. Sci. U.S.A.* **2008**, *104*, 6885–6892.
(2) Edwards, P. P.; Meurig, T. *Angew. Chem.* **2007**, *46*, 5480–5486.
(3) Mulvaney, P. L. *Langmuir* **1996**, *12*, 788–800.
(4) Ni, W.; Kou, X.; Yang, Z.; Wang, J. *ACS Nano* **2008**, *2*, 677–686.
(5) Wang, H.; Halas, N. J. *Adv. Mater.* **2008**, *20*, 820–825.
(6) Link, S.; El-Sayed, M. A. *Int. Rev. Phys. Chem.* **2000**, *19*, 409–453.
(7) Ghosh, S. K.; Pal, T. *Chem. Rev.* **2007**, *107*, 4797–4862.
(8) Kelly, K. L.; Coronado, E.; Zhao, L. L.; Schatz, G. C. *J. Phys. Chem. B* **2003**, *107*, 668–677.
(9) Xia, Y.; Halas, N. J. *MRS Bull.* **2005**, *30*, 338–343.
(10) Sherry, L. J.; Jin, R.; Mirkin, C. A.; Schatz, G. C.; Van Duyne, R. P. *Nano Lett.* **2006**, 2060–2065.
(11) Lieberman, I.; Shemer, G.; Fried, T.; Kosower, E. M.; Markovich, G. *Angew. Chem.* **2008**, *47*, 4855–4857.
(12) Toftegaard, R.; Arnbjerg, J.; Daasbjerg, K.; Ogilby, P. R.; Dmitriev, A.; Sutherland, D. S.; Poulsen, L. *Angew. Chem.* **2008**, *47*, 6025–6027.
(13) Lal, S.; Westcott, S. L.; Taylor, R. N.; Jackson, J. B.; Nordlander, P.; Halas, N. J. *J. Phys. Chem. B* **2002**, *106*, 5609–5612.
(14) Shimada, T.; Ookubo, K.; Komuro, N.; Shimizu, T.; Uehara, N. *Langmuir* **2007**, *23*, 11225–11232.
(15) Elghanian, R.; Storhoff, J. J.; Mucic, R. C.; Letsinger, R. L.; Mirkin, C. A. *Science* **1997**, *277*, 1078–1080.
(16) Bailey, R. C.; Nam, J.-M.; Mirkin, C. A.; Hupp, J. T. *J. Am. Chem. Soc.* **2003**, *125*, 13541–13547.
(17) Lapokto, D. O.; Lukianova-Helb, E. Y.; Oraevsky, A. O. *Nanomedicine* **2007**, *2*, 241–253.
(18) Loo, C.; Lin, A.; Hirsch, L.; Lee, M.-H.; Barton, J.; Halas, N. J.; West, J.; Drezek, R. *Tech. Cancer Res. Treat.* **2004**, *3*, 33–40.
(19) Zijlstra, P.; Tchebotareva, A. L.; Chon, J. W. M.; Gu, M.; Orrit, M. *Nano Lett.* **2008**, *8*, 3493–3497.
(20) Kulzer, F.; Laurens, N.; Besser, J.; Schmidt, T.; Orrit, M.; Spaink, H. P. *ChemPhysChem* **2008**, *9*, 1761–1766.
(21) Van Dijk, M. A.; Lippitz, M.; Orrit, M. *Acc. Chem. Res.* **2005**, *38*, 594–601.
(22) Boyer, D.; Tamarat, P.; Maali, A.; Lounis, B.; Orrit, M. *Science* **2002**, *297*, 1160–1163.
(23) Diagaradjane, P.; Shetty, A.; Wang, J. C.; Elliott, A. M.; Schwartz, J.; Shentu, S.; Park, H. C.; Deorukhkar, A.; Stafford, R. J.; Cho, S. H.; Tunnell, J. W.; Hazle, J. D.; Krishnan, S. *Nano Lett.* **2008**, *8*, 1492–1500.
(24) Lapotko, D. O.; Lukianova, E.; Potapnev, M.; Aleinikova, O.; Oraevsky, A. *Cancer Lett.* **2006**, *239*, 36–45.
(25) O'Neal, D. P.; Hirsch, L. R.; Halas, N. J.; Payne, J. D.; West, J. L. *Cancer Lett.* **2004**, *209*, 171–176.
(26) Averitt, R. D.; Sakar, D.; Halas, N. J. *Phys. Rev. Lett.* **1997**, *78*, 4217–4220.
(27) Oldenberg, S. J.; Averitt, R. D.; Westcott, S. L.; Halas, N. J. *Chem. Phys. Lett.* **1998**, *28*, 243–247.
(28) Hirsch, L.; Stafford, R. J.; Bankson, J. A.; Sershen, S. R.; Rivera, B.; Prince, R. E.; Hazle, J. D.; Halas, N. J.; West, J. L. *Proc. Natl. Acad. Sci. U.S.A.* **2003**, *100*, 13549–11354.
(29) Wang, X.; Lin, K. S. K.; Chan, J. C. C.; Chen, S. *Chem. Commun.* **2004**, 2762–2763.
(30) Giesbers, M.; Kleijn, J. M.; Cohen Stuart, M. A. *J. Colloid Interface Sci.* **2002**, *252*, 138–148. Etienne, M.; Walcarius, A. *Talanta* **2003**, *59*, 1173–1188. Howarter, J. A. *Langmuir* **2006**, *22*, 11142–11147.
(31) Abbruzzetti, S.; Crema, E.; Masino, L.; Vecli, A.; Viappiani, C.; Small, J. R.; Libertini, L. J.; Small, E. W. *Biophys. J.* **2000**, *78*, 405–415.
(32) Abbruzzetti, S.; Viappiani, C.; Small, J. R.; Libertini, L. J.; Small, E. W. *Biophys. J.* **2000**, *79*, 2714–2721.
(33) Abbruzzetti, S.; Viappiani, C.; Murgida, D. H.; Erra-Balsells, R.; Bilmes, G. M. *Chem. Phys. Lett.* **1999**, *304*, 167–172.
(34) Braslavsky, S. E.; Heibel, G. E. *Chem. Rev.* **1992**, *92*, 1381–1410.
(35) Gensch, T.; Viappiani, C.; Braslavsky, S. E. In *Encyclopedia of spectroscopy and spectrometry*; Lindon, J. C., Tranter, G. E., Holmes, J. L., Eds.; Academic Press Ltd: London, 1999; pp 1124−1132.
(36) Gensch, T.; Viappiani, C. *Photochem. Photobiol. Sci.* **2003**, *2*, 699–721.
(37) Small, J. R. In *Numerical Computer Methods*; Brand, L., Johnson, M. L., Eds.; Academic Press, Inc.: SanDiego, 1992; Vol. 210, pp 505−521.

(38) Small, J. R.; Libertini, L. J.; Small, E. W. *Biophys. Chem.* **1992**, *42*, 24–48.
(39) Tran, M. L.; Centeno, S. P.; Hutchison, J. A.; Engelkamp, H.; Liang, D.; Van Tendeloo, G.; Sels, B. F.; Hofkens, J.; Uji-i, H. *J. Am. Chem. Soc.* **2008**, *130*, 17240–17241.
(40) Prodan, E.; Nordlander, P. J. C. P. *J. Chem. Phys.* **2004**, *120*, 5444–5454.
(41) Link, S.; El-Sayed, M. A. *J. Phys. Chem. B* **1999**, *103*, 8410–8426.
(42) Cao, L.; Barsic, D. N.; Guichard, A. R.; Brongersma, M. L. *Nano Lett.* **2007**, *7*, 3523–3527.
(43) Cotlet, M.; Hofkens, J.; Maus, M.; Thomas Gensch, T.; Van der Auweraer, M.; Michiels, J.; Dirix, G.; Van Guyse, M.; Vanderleyden, J.; Visser, A. J. W. G.; De Schryver, F. C. *J. Phys. Chem. B* **2001**, *105*, 4999–5006.
(44) Haupts, U.; Maiti, S.; Schwille, P.; Webb, W. W. *Proc. Natl. Acad. Sci. U.S.A.* **1998**, *95*, 13573–13578.
(45) Chen, Y.; Mueller, J. D.; Ruan, Q. Q.; Gratton, E. *Biophys. J.* **2002**, *82*, 133–144.

JP810544B